Reaction Paths of CO Insertion into the Pt^{II}–CH_3 Bond. An MO Study

Shigeyoshi Sakaki,*[1a] Kazuo Kitaura,[1b,c] Keiji Morokuma,[1b] and Katsutoshi Ohkubo[1a]

Contribution from the Department of Synthetic Chemistry, Faculty of Engineering, Kumamoto University, Kurokami, Kumamoto 860, Japan, and the Institute for Molecular Science, Myodaiji, Okazaki 444, Japan. *Received September 16, 1982*

Abstract: The bonding nature and relative stability of $Pt(CH_3)F(CO)(PH_3)$ and $Pt(COCH_3)F(PH_3)$, the reactant and the product of CO insertion, were theoretically studied. The Pt–CH_3 bond in $Pt(CH_3)F(CO)(PH_3)$ is stronger in the structure where CH_3 is trans to PH_3 (**1**) than in the structure where CH_3 is trans to F (**2**). For $Pt(COCH_3)F(PH_3)$, the Y-shaped form is the least stable and is not a local minimum. In the most stable T-shaped structure, F and PH_3 are trans to each other, the fact explainable in terms of the trans-influence effect. Furthermore, all of the probable reaction paths of the CO insertion were examined. The CH_3 migration is an easy path in both reaction systems **1** and **2**, and the concerted move of CO and CH_3 concurrent with the ∠FPtP opening is easy in **1** but difficult in **2**, whereas the CO migration is difficult in both **1** and **2**. The factors determining the choice of reaction paths were presented.

The carbonyl insertion reaction into a metal–alkyl bond is a key step in many catalytic reactions of transition-metal complexes, such as oxo reaction, Reppe reaction, and various related reactions[2] and, therefore, has been studied actively. One of the purposes of such studies is to answer questions about the course of reaction.[2-5] There are three possible reaction mechanisms: the alkyl migration (eq 1),[3] the CO migration (eq 2),[4] and the concerted migration of CO and alkyl with opening the LML′ angle (eq 3),[5] as shown in Scheme I. The alkyl migration has been established experimentally in Mn(I) complexes,[3a,b,d] while the other two mechanisms have been postulated on the basis of the geometry of products.[4,5]

Theoretical studies are expected to answer which of the three is most likely and why it is so. Furthermore, they may offer a variety of information about intermediates, the reaction mechanism, and the catalytic role of metal in this reaction. Nevertheless, theoretical work on the system is virtually nonexistent except for the work by Berke and Hoffmann,[6] in which the details of the course of reaction have not been fully investigated.

In the present paper we intend to carry out a theoretical investigation of the CO insertion to reveal the structure and bonding nature of the intermediates, the effect of different ligands and metals on the reactivity, and especially the course of reaction. We will examine the CO insertion in $Pt(CH_3)F(CO)(PH_3)$ as a model of the real system, $PtX(R)(CO)(PR'_3)$ (X = halogen; R = CH_3, C_6H_5, etc.; R′ = Ph, etc.)[7-10] The choice of the system is based on the following reasons. (i) The rate-determining step is insensitive to the solvent and the incoming ligand.[2e,7,8b,11] (ii) A

Scheme I

Alkyl-migration

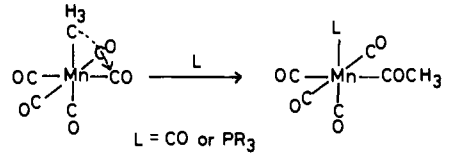

(1)

CO-migration

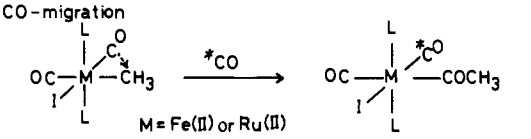

(2)

Concerted migration of CO and Alkyl with opening of LIrCl Angle

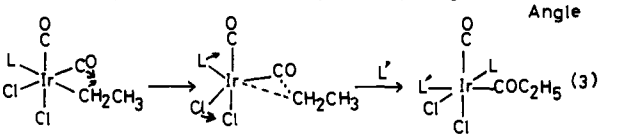

(3)

critical ligand effect on the reactivity has been reported;[10] when the tertiary phosphine ligand is placed at the trans position of the alkyl ligand, the CO insertion takes place, but, when the halogen ligand is positioned trans to the alkyl ligand, the insertion does not take place. It is of considerable interest to explain theoretically this ligand effect. (iii) A primary product is considered to be the three-coordinate acetyl complex, $PtX(COR)(PR'_3)$.[7,8,9b,10b,c,11]

$$PtX(R)(CO)(PR'_3) \rightarrow PtX(COR)(PR'_3) \qquad (4)$$

Three coordinate complexes such as this play an important role in many catalytic reactions of transition-metal ions,[3c,12-16] and thus, it is worthwhile to investigate its structure and coordinate bonding nature. (iv) The CO insertion of d^8 planar complexes is important in the catalytic chemistry. For exampdle, palladium(II) complexes offer various interesting catalytic reactions in which the carbonyl insertion is often involved as a key step.[2,9,11,17] Through this MO

(1) (a) Kumamoto University. (b) Institute for Molecular Science. (c) Present address: Osaka City University.

(2) (a) Taqui Khan, M. M.; Martell, A. E. "Homogeneous Catalysis by Metal Complexes"; Academic Press: New York, 1974; Vol. I and II. (b) Wender, I.; Pino, P. "Organic Synthesis via Metal Carbonyls"; Wiley-Interscience: New York, 1977; Vol. I and II. (c) Cornils, B. "New Synthesis with Carbon Monoxide"; Falbe, J., Ed.; Springer-Verlag: New York, 1980; p 1. (d) Mullen, A., ref 2d, p 243. (e) Calderazzo, F. *Angew. Chem., Int. Ed. Engl.* **1977**, *16*, 299.

(3) (a) Noack, K.; Calderazzo, F. *J. Organomet. Chem.* **1967**, *10*, 101. (b) Noack, K.; Ruch, M.; Calderazzo, F. *Inorg. Chem.* **1968**, *7*, 345. (c) Ozawa, F.; Yamamoto, A. *Chem. Lett.* **1981**, 289. (d) Flood, T. C.; Jensen, J. E.; Statler, J. A. *J. Am Chem. Soc.* **1981**, *103*, 4410.

(4) Pânkowski, M.; Bigorgne, M. "Abstract of Papers", 8th International Conference on Organometallic Chemistry, Kyoto, Japan, 1977; 5B02; *J. Organomet. Chem.* **1971**, *30*, 227. Brunner, H.; Vogt, H. "Abstract of Papers", 10th International Conference on Organometallic Chemistry, Toronto, Canada, 1981; p 103.

(5) Glyde, R. W.; Mawby, R. J. *Inorg. Chim. Acta* **1971**, *5*, 317.

(6) Berke, H.; Hoffmann, R. *J. Am. Chem. Soc.* **1978**, *100*, 7224.

(7) Glyde, R. W.; Mawby, R. J. *Inorg. Chem.* **1971**, *10*, 854.

(8) (a) Wilson, C. J.; Green, M.; Mawby, R. J. *J. Chem. Soc., Dalton Trans.* **1974**, 421. (b) *Ibid.* **1974**, 1293.

(9) (a) Garrow, P. E.; Heck, R. F. *J. Am. Chem. Soc.* **1976**, *98*, 4115. (b) Sugita, N.; Minkiewicz, J. V.; Heck, R. F. *Inorg. Chem.* **1978**, *17*, 2809.

(10) (a) Anderson, G. K.; Cross, R. J. *J. Chem. Soc., Chem. Commun.* **1978**, 819; (b) *J. Chem. Soc., Dalton Trans.* **1979**, 1246; (c) **1980**, 712, 1434.

(11) Romeo, R.; Uguagliati, P.; Belluco, U. *J. Mol. Catal.* **1975/76** *1*, 325 and references cited therein.

(12) Komiya, S.; Albright, T. A.; Hoffmann, R.; Kochi, J. K. *J. Am. Chem. Soc.* **1976**, *98*, 7255.

(13) Thorn, D. L.; Hoffmann, R. *J. Am. Chem. Soc.* **1978**, *100*, 2079.

(14) Dedieu, A. *Inorg. Chem.* **1980**, *19*, 375.

(15) Kitaura, K.; Morokuma, K. 28th Synposium on Organometallic Chemistry, Japan, 1981; p 7.

(16) McCarthy, T. J.; Nuzzo, R. G.; Whiteside, G. M. *J. Am. Chem. Soc.* **1981**, *103*, 1676.

(17) (a) Maitlis, P. M. "The Organic Chemistry of Palladium"; Academic Press: New York, 1971; Vol. 2. (b) Jolley, P. W.; Wilke, G. "The Organic Chemistry of Nickel"; Academic Press: New York, 1975; Vol. II.

0002-7863/83/1505-2280$01.50/0

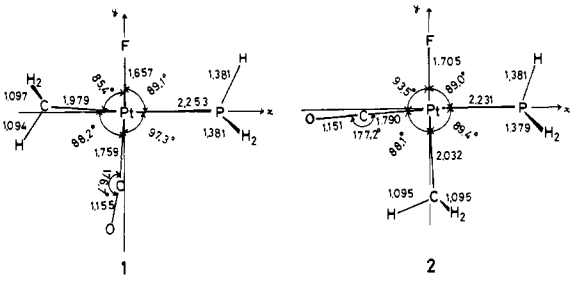

Figure 1. Optimized geometries of $PtF(CH_3)(CO)(PH_3)$ in units of Å and deg.

study, we hope (a) to answer the question regarding the course of reaction, i.e., to reveal which of the three migrations, alkyl (eq 1), CO (eq 2), or concerted (eq 3), is in operation and to elucidate a factor determining the choice, (b) to explain theoretically the ligand effect on the reactivity described above, and (c) to offer for three-coordinate platinum(II)–acyl complexes some theoretical information such as the structure, the relative stability of various isomers, and the coordinate bonding nature.

Computational Details: Geometry and Reaction Coordinate of CO Insertion

Ab-initio Hartree–Fock calculations were carried out on reaction 4 with the IMSPACK program,[18] where PH_3 and F were used as models for the tertiary phosphine and the halogen ligands and R = CH_3. For the Pt atom, the effective relativistic core potential of Topiol et al. was employed with a valence basis set [3s 2p 2d] contracted from (3s 3p 4d) primitives.[19] For ligand atoms, the STO-2G[20a,b] and the 3-21G[20c] basis sets were employed for geometry optimization and for energetics and bonding nature, respectively.

In the present study we carried out only the restricted Hartree–Fock calculation for the closed-shell singlet state. The closed-shell singlet should be able to describe qualitatively the electronic structure of this reaction system, since it is well established that Pt^{II} complexes are in a low-spin d^8 electron configuration. Considering the size of the system, we have not performed CI calculation. Therefore, the calculated energetics presented here including the reaction barriers should be taken only qualitatively.

The geometries of two isomers, **1** and **2** (Figure 1), of the reactant $PtF(CH_3)(CO)(PH_3)$ were fully optimized by means of the energy gradient method.[21] Equilibrium geometries of three-coordinate acetyl complex $PtF(COCH_3)(PH_3)$, the product of the carbonyl insertion reaction, were searched for several isomers **3**–**6**. The structures of isomers **4** and **5** were fully optimized with the constraint of the C_s symmetry. A small deviation from the C_s-optimized structures creates a force that tries to retain the C_s symmetry, and hence **4** and **5** are equilibrium geometries; in fact, the perpendicular structures of **4** and **5** are more unstable than the corresponding in-plane structures by ca. 2 and 9 kcal/mol, respectively. The structures of **3** and **6** could not be optimized; the optimization starting from either of them ended up at the structure **5**. Nevertheless, MO calculations of **3** and **6** were carried out for the assumed structures; the structure of **6** was assumed to be an ideal Y-shaped structure with the three bond angles around Pt of 120°, where the bond length and intraligand bond angles were taken to be the average of **4** and **5**. The structure of **3** was taken to be a slightly distorted T-shaped structure, where only ∠PPtF was optimized to be 110° by the 3-21G energy calculation and the other geometrical parameters were taken to be the same as those of **5**.

Scheme II

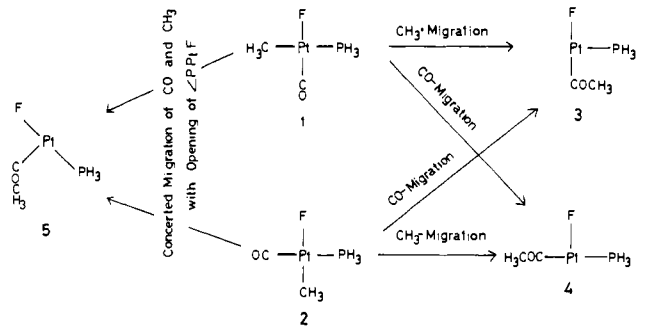

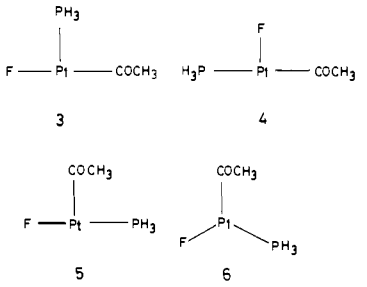

Next, mutual isomerizations among these isomers were investigated. The top of the barrier of isomerization was searched with STO-2G energy calculations, where geometrical parameters were assumed as follows. In the isomerization **3** → **4**, the optimized geometrical parameters of **4** were used and the energy maximum was searched by changing only ∠PPtC as the reaction coordinate; in the isomerization **3** → **5**, the optimized geometrical parameters of **5** were adopted and the ∠PPtF was used as the reaction coordinate, only when 3-21G energy calculation was done because STO-2G calculation gave no barrier; in the isomerization **4** → **5**, the geometrical parameters were smoothly varied between those of **4** and those of **5**, and the ∠FPtP was taken as a reaction coordinate; and in the isomerizations **6** → **3**, **6** → **4**, and **6** → **5**, the geometrical parameters of **3**, **4**, or **5** were used, respectively, and two angles, for example, ∠FPtC and ∠FPtP in the **6** → **4** isomerization, were simultaneously varied. The energy of a single 3-21G calculation at the top of the potential barrier was used for energetics.

Finally, all possible courses of the CO insertion were examined, where the T-shaped acetyl complexes **3**, **4**, and **5** were considered to be the products as described later. As shown in Scheme II, **1** isomerizes to **3** through CH_3 migration and to **4** through CO migration and **2** is converted into **3** through CO migration and into **4** through CH_3 migration. Although **5** cannot be formed directly from **1** and **2** through either CO or CH_3 migration, it should be included as a product. Possible courses of reaction to **5** from **1** are CH_3 migration (**1** → **3**) followed by F migration (**3**

(18) Morokuma, K.; Kato, S.; Kitaura, K.; Ohmine, I.; Sakai, S.; Obara, S. IMS Computer Center Library program, **1980**, *0372*.
(19) Basch, H.; Topiol, S. *J. Chem. Phys.* **1979**, *71*, 802.
(20) (a) Hehre, W. J.; Stewart, R. F.; Pople, J. A. *J. Chem. Phys.* **1969**, *51*, 2657. (b) Hehre, W. J.; Ditchfield, R.; Stewart, R. F.; Pople, J. A. *Ibid.* **1970**, *52*, 2769. (c) Binkley, J. S.; Pople, J. A.; Hehre, W. J. *J. Am. Chem. Soc.* **1980**, *102*, 939.
(21) (a) Pulay, P. "Modern Theoretical Chemistry"; Schaefer, III, Ed.; Plenum: New York, 1977; p 153. (b) Kitaura, K.; Obara, S.; Morokuma, K. *Chem. Phys. Lett.* **1981**, *77*, 452.
(22) Clark, H. C.; Corfield, P. W. R.; Dixon, K. R.; Ibers, J. A. *J. Am. Chem. Soc.* **1967**, *89*, 3360.
(23) Manojlović-Muir, L.; Muir, K. W.; Walker, R. *J. Chem. Soc., Dalton Trans.* **1976**, 1279.
(24) Field, J. S.; Wheatley, P. J. *J. Chem. Soc., Dalton Trans.* **1974**, 702.
(25) Badley, E. M.; Sim, G. A., to be published, cited in: Badley, E. M.; Chatt, J.; Richards, R. L.; Sim, G. A. *J. Chem. Soc. D* **1969**, 1322.
(26) Orchin, M.; Schmidt, P. J. *Coord. Chem. Rev.* **1968**, *3*, 345.
(27) Russell, D. R.; Tucker, P. A.; Wilson, S. *J. Organomet. Chem.* **1976**, *104*, 387.
(28) Day, C. S.; Day, V. W.; Shaver, A.; Clark, H. C. *Inorg. Chem.* **1981**, *20*, 2188.
(29) Ibott, D. G.; Payne, N. C.; Shaver, A. *Inorg. Chem.* **1981**, *20*, 2193.
(30) (a) Bartlett, N.; Lohmann, D. H. *Proc. Chem. Soc., London* **1962**, 115; *J. Chem. Soc.* **1962**, 5253. (b) Ibers, J. A.; Hamilton, W. C. *J. Chem. Phys.* **1965**, *44*, 1748.
(31) Bartlett, N.; Einstein, F.; Stewart, D. F.; Trotter, J. *J. Chem. Soc. A* **1967**, 1190.
(32) Mellor, D. P.; Stephenson, N. C. *Aust. J. Sci. Res., Ser. A* **1951**, *A4*, 406.

Table I. Comparison of Optimized and Experimental Bond Lengths

	complex	bond length calcd	bond length exptl	
Pt-P	1	2.25	2.34	*trans*-$PtCl(CO)(PEt_3)_2$[22]
			2.35	
	2	2.23	2.282	*cis*-$PtCl_2(CO)(PPh_3)_2$[23]
			2.30	*trans*-$Pt(p\text{-}ClC_6H_4)(CO)(PEt_3)_2$[24]
	4	2.34		
	5	2.21		
Pt-CO	1	1.76	1.75	*cis*-$PtCl_2(CO)(PEt_3)_2$[25]
	2	1.79	1.78	*trans*-$PtCl_2(CO)(ONC_6H_4OMe)$[26]
			1.858	*cis*-$PtCl_2(CO)(PPh_3)$[23]
			1.82	$PtCl_3(CO)^-$[27]
C-O	1	1.16	1.14	*trans*-$PtCl(CO)(PEt_3)_2$[22]
	2	1.15	1.114	*cis*-$PtCl_2(CO)(PPh_3)_2$[23]
			1.06	*trans*-$Pt(p\text{-}ClC_6H_4)(CO)(PEt_3)_2$[24]
			1.12	$PtCl_3(CO)^-$[27]
$Pt-CH_3$	1	1.98	2.06	$Pt(CH_3)(1.5\text{-}COD)(\eta^1\text{-}Cp)$[28]
	2	2.03	2.054	$Pt(CH_3)(COD)(7\text{-}\eta\text{-}C_9F_6H_5)$[29]
Pt-F	1	1.66	1.74	PtF_6^-[30a]
	2	1.71	1.82-1.83	PtF_6^-[30b]
			1.89	PtF_6^{2-}[31]
	4	1.61	1.91	PtF_6^{2-}[32]
	5	1.62		
$Pt-COCH_3$	4	1.93	1.972	$Pt_2(\mu\text{-}Cl)_2(COC_2H_5)_2(PMe_2Ph)_2$[33]
	5	1.91		
C-O of $COCH_3$	4	1.23	1.208	$Pt_2(\mu\text{-}Cl)_2(COC_2H_5)_2(PMe_2Ph)_2$[33]
	5	1.22		
C-C	4	1.56	1.526	$Pt_2(\mu\text{-}Cl)_2(COC_2H_5)_2(PMe_2Ph)_2$[33]
	5	1.56		

→ **5**), CO migration (**1** → **4**) followed by PH_3 migration (**4** → **5**), and the direct concerted migration CO and CH_3 accompanied by ∠PPtF opening. Possible courses of reaction **2** → **5** are CH_3 migration (**2** → **4**) followed by the PH_3 migration (**4** → **5**), CO migration (**2** → **3**) followed by F migration (**3** → **5**), and the concerted migration. The reaction involving the PH_3 migration seems unlikely, as it is usually a difficult process (see later). Here we tentatively call the **1** or **2** → **5** process the concerted migration.

For examination of all of the above-mentioned courses of reaction, the $(CO)Pt(CH_3)$ angle was taken to be a reaction coordinate and fixed at various values, for each of which the Pt–CH_3 bond length, the orientation of CO and CH_3 ligands, and positions of F and PH_3 were optimized. The Pt–F, Pt–PH_3, Pt–CO, C–O, C–H, and P–H bond lengths and the HPH and HCH angles were assumed to vary smoothly from the reactant to the product. Optimizations were carried out by a parabolic fit for each geometrical parameter. At each optimized geometries for a given $\angle(CO)Pt(CH_3)$ an MO calculation using the 3-21G basis set for ligand atoms was performed for energetics and bonding nature. Details in the geometrical changes will be given latter in Figures 5 and 6.

Results and Discussion

Structures of $Pt(CH_3)F(CO)(PH_3)$. The optimized structures of two isomers of $Pt(CH_3)F(CO)(PH_3)$ are shown in Figure 1. As shown in Table I, the calculated Pt–CO and Pt–CH_3 bond lengths agree well with the corresponding experimental values, and the calculated Pt–PH_3 bond lengths are in the range of various known Pt–tertiary phosphine bond lengths. The calculated Pt–F bond lengths are too short, in comparison with the experimental Pt^{IV}–F and Pt^{V}–F bond lengths. This discrepancy is perhaps because the anionic F^- ligand is not represented satisfactorily by the compact STO-2G basis set. Total energies and overlap populations are shown in Table II. Isomer **1** is more stable than **2**, which can be attributed to a stronger Pt–CO bond in **1** than that in **2**. The stronger Pt–CO bond of **1** is due to the trans-positioned F ligand. The F ligand has weak σ-donating and moderate π-donating ability, facilitating both the σ-donation from CO and the π back donation to CO. As a result, **1** has a stronger Pt–CO bond and becomes more stable than **2**. The Pt–CH_3 bond strength of **1** is slightly weaker than that of **2**, as expected from the strong trans-influence effect of PH_3.

Table II. Total Energies and Mulliken Overlap Population of $PtF(CH_3)(CO)(PH_3)$

	1	2
E_{tot}, hartree	−618.5328	−618.5127
E_{rel}, kcal/mol	0.0	+13
Pt-F	0.12	0.13
Pt-PH_3	0.20	0.29
Pt-CO	0.43	0.31
Pt-CH_3	0.28	0.31

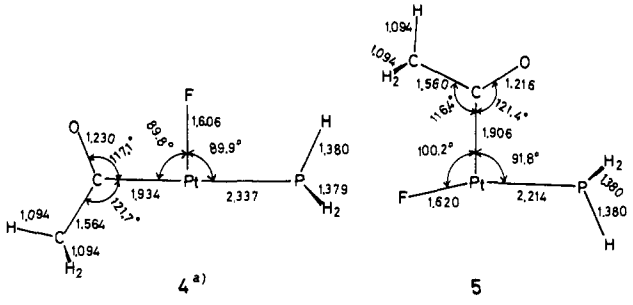

Figure 2. Optimized geometries of $PtF(COCH_3)(PH_3)$ in units of Å and deg. (a) Though the structure of **4** may not correspond to the grobal minimum, this is most likely for the structure of product.

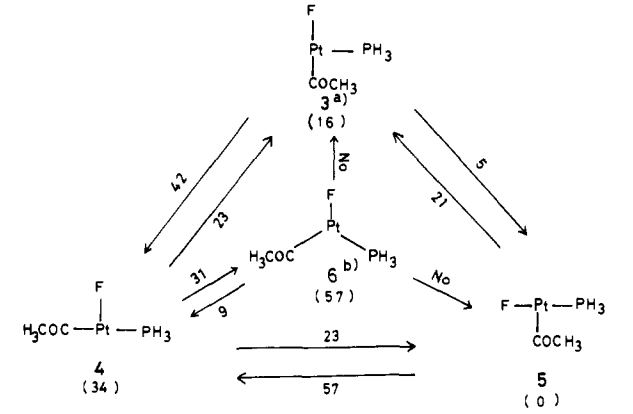

Figure 3. Relative stability of several isomers of three-coordinate $PtF(COCH_3)(PH_3)$ and potential barriers for mutual isomerization: numbers in parentheses represent the energy of the complex relative to the most stable complex (**5**) (kcal/mol); numbers near the arrows represent the potential barrier necessary for the isomerization presented by the arrow (kcal/mol). (a) ∠PPtF = 100°. Other geometrical parameters were taken to be the same as those of **5**. (b) ∠FPtP = ∠FPtC = 120°.

Structure and Isomerization of Three-Coordinate $Pt(COCH_3)F(PH_3)$. The optimized structures of **4** and **5** are shown in Figure 2. Apparently, **4** has an ideal T-shaped structure, while **5** has a distorted T-shaped structure. As shown in Table I, the calculated Pt–$COCH_3$ distance is slightly smaller than experiment,[33] while the calculated intraligand distances such as C–O and C–C are slightly longer than experiment.[33] **4** has longer Pt–PH_3 and Pt–$COCH_3$ distances than **5**, perhaps because PH_3 and $COCH_3$, both possessing strong trans-influence ability, are positioned trans to each other in **4**.

Next the mutual isomerization of isomers **3**–**6** was examined, and the relative stability of isomers and the barriers of isomerization are shown in Figure 3. The following characteristic features are found. (1) The Y-shaped isomer **6** is the most unstable and isomerizes to **3** or **5** with no barrier; i.e., **6** is not a local minimum. (2) The relative stability of the T-shaped isomers decreases in the order **5** > **3** > **4**. (3) The isomerization **3** → **5** proceeds with little barrier, isomerizations **5** → **3**, **4** → **3**, and **4** → **5** proceed with a moderate barrier, and isomerizations **3** → **4** and **5** → **4** require

(33) Anderson, G. K.; Cross, R. J.; M-Muir, L.; Muir, K. W.; Solomon, T. *J. Organomet. Chem.* **1979**, *170*, 385.

Scheme III

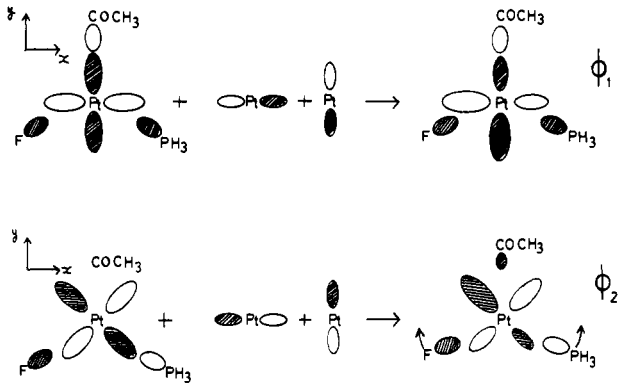

a high potential barrier. Though the absolute barrier heights are expected to be overestimated and should not be taken quantitatively (vide supra), these results suggest that **4** and **5** are possible products of the CO insertion reaction. Although **3** isomerizes to **5** easily, **3** should be included in the products, for it is the direct product of CH_3 migration from **1** and of CO migration from **2** (Scheme II). The calculated relative stability of isomers **3**–**5** is consistent with the known order of the trans-influence effect: $COCH_3^- > PR_3 >$ halogen, which is deduced from $PPh_3 >$ halogen in Pt^{II} complexes,[34] $COC_2H_5^- > PMe_3$ in Hg^{II} complexes,[34] and $COCH_3^- > CH_3^-$, $CH_3^- > PR_3$ in Ir^{III} and Rh^{III} complexes,[35] respectively. In **4**, the empty coordinate site is at the trans position to the weakest F^- ligand, and the strongest $COCH_3^-$ ligand is trans to the second-strongest PH_3 ligand. Thus, **4** is the most unstable. In **3**, the empty site is trans to the second-strongest PH_3 ligand and the strongest $COCH_3^-$ ligand is trans to the weakest F^- ligand. In **5**, the empty site is trans to the strongest $COCH_3^-$ ligand and the weakest F^- ligand is trans to the second-strongest PH_3 ligand. Consequently, the relative stability of T-shaped complexes should increase in the order **4** < **3** < **5**.

The instability of the Y-shaped complex **6** can be understood by considering the orbital energies of MO's ϕ_1 and ϕ_2 (Scheme III). If the strongest ligand $COCH_3^-$ is placed on the y axis, ϕ_1 will be destabilized more than ϕ_2, i.e., ϕ_1 becomes LUMO and ϕ_2 becomes HOMO. Therefore it is sufficient to examine the energy of ϕ_2. As is schematically depicted in Scheme III, ϕ_2 is mainly composed of the Pt d_{xy} orbital. Though the Pt p_x orbital mixes in a bonding way with PH_3 and F^- ligands and the Pt p_y orbital also mixes into d_{xy} in a bonding way with strong $COCH_3^-$ and PH_3 ligands, the d_{xy} orbital still dominates the following discussion. When PH_3 and F^- ligands moves in the direction of the arrows shown in Scheme III, the antibonding interaction between the d_{xy} orbital and the F^- and PH_3 ligand orbitals is reduced and ϕ_2 becomes lower in energy. Consequently, the T-shaped structure **5** with the $COCH_3$ in the middle becomes the most stable. Structure **3**, where the stronger ligand PH_3 moves in the direction of the arrow and F^- opposite to the arrow, is less stable than **5**, and structure **4**, where the weakest ligand F^- moves in the direction of the arrow and the stronger PH_3 opposite to the arrow, is the least stable. This situation is slightly different from $Au(CH_3)_3^-$ to which Hoffmann et al. offered an explanation.[12] There the complex had degenerated half-ocupied HOMO's ϕ_1 and ϕ_2 in the Y structure, and the Jahn–Teller effect explained the Y → T deformation.

Courses of the CO Insertion Reaction. Now, let us examine the CO insertion leading to the Pt^{II}–acetyl complex **3**, **4**, or **5**. The $(CH_3)Pt(CO)$ angle was taken as a reaction coordinate as described above. Total energies and geometries along the partially optimized paths of reaction are shown in Figure 4 and 5. Since the $(CH_3)Pt(CO)$ angle in the reactants is about 88° for both **1**

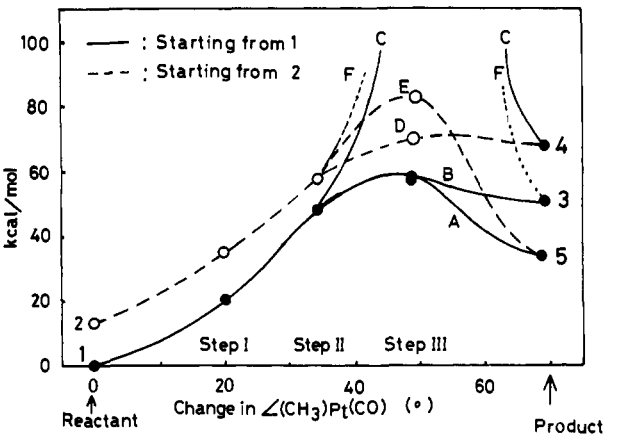

Figure 4. Energy changes along various courses of CO insertion reaction. A–F correspond to A–F of Figure 5 and Scheme IV.

Scheme IV

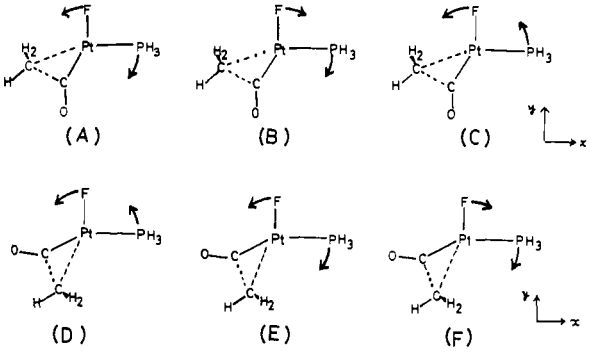

Scheme V

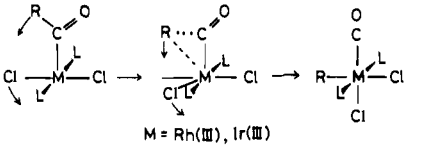

and **2**, steps I, II, and III correspond to angles of 68°, 53°, and 39°, respectively. First, we will follow the reaction starting from **1**. The most stable courses of reaction, marked A and B in Figures 4 and 5, both have an activation energy of ca. 60 kcal/mol. In course A, the FPtP angle opens up as shown in Scheme IVA, and structure **7** at step III (Figure 5) looks like product **5** (Figure 2). Thus, this course of reaction leads to **5** and can be called either the CH_3 migration followed by F migration, noting ∠FPt(CO) ~ 90°, or the concerted migration. Though it is rather arbitary to choose one of the above, the latter seems more reasonable; the long C–C bond and the large FPtP angle of **7** suggest that the ∠FPtP opening is concurrent with the C–C bond formation. A similar reaction has been proposed for the deacylation of $MCl_2(COR)L_2$ (M = Rh^{III} or Ir^{III}; R = CF_nH_{3-n}, n = 0–3; L = tertiary phosphine)[35b,36] and the CO insertion of $IrCl_2Et(CO)_2L'$ (L' = $AsMe_{3-n}Ph_n$, n = 1,2),[5] as shown in Schemes V and I, respectively. In the former, the CH_3 migration is to take place via a concerted movement of the Cl ligand and the CH_3 group, in which Cl migrates to the vacant apical site of the square pyramid and CH_3 to the newly formed vacant site. In the latter, the concerted movement of CO and C_2H_5 is to occur while ∠ClIrL' opens up simultaneously, and consequently a vacant site is formed at the trans position of the COC_2H_5 group formed.

In course B, the step III geometry is optimized upon keeping ∠FPtP = 90° and structure **8** of Figure 5 is obtained, which is slightly less stable relative to **7** in course A. Though ∠PPt(CO)

(34) Appleton, T. G.; Clark, H. C.; Manger, L. E. *Coord. Chem. Rev.* **1973**, *10*, 335.
(35) (a) Blake, D. M.; Winkelman, A.; Chung, Y. L. *Inorg. Chem.* **1975**, *14*, 1326. (b) Bennett, M. A.; Jeffery, J. C.; Robertson, G. B. *Ibid.* **1981**, *20*, 323.
(36) (a) Kampmeier, J. A.; Rodehoast, R. M.; Philip, J. B., Jr. *J. Am. Chem. Soc.* **1981**, *103*, 1847. (b) Egglestone, D. L.; Baird, M. C.; Loch, C. J. L.; Turner, G. *J. Chem. Soc., Dalton Trans.* **1977**, 1576.

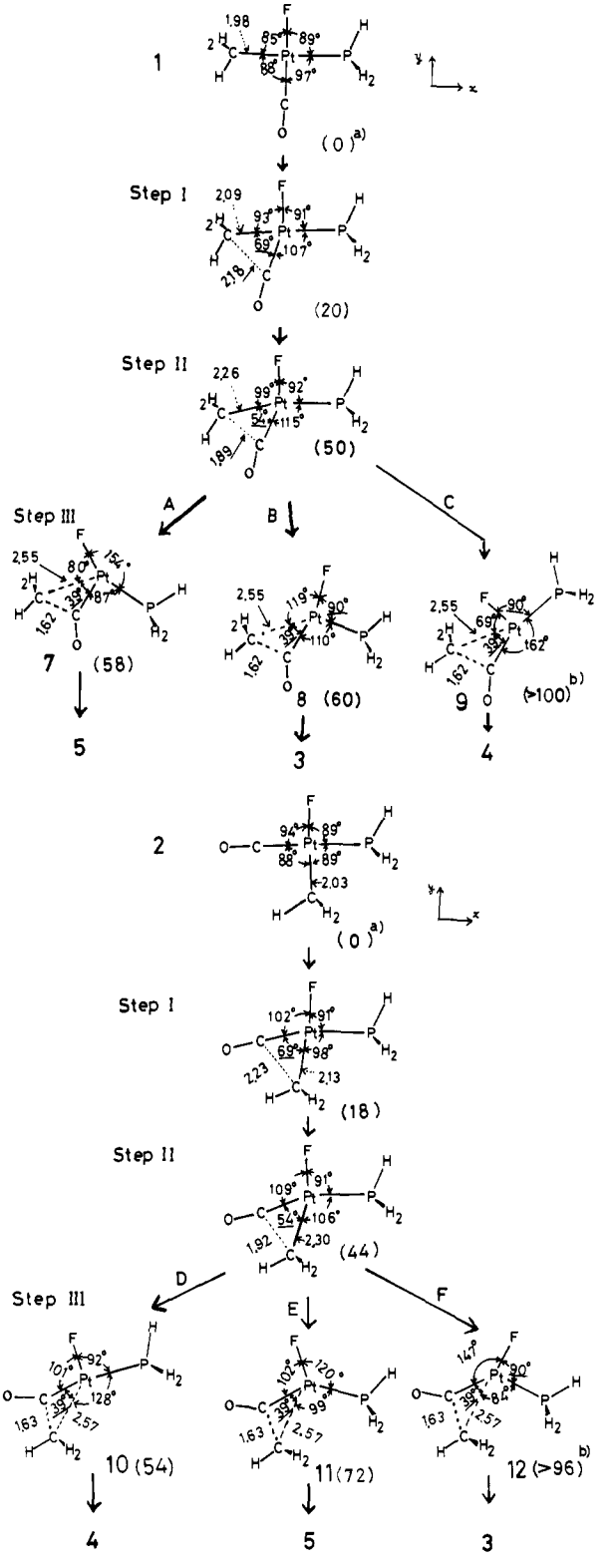

Figure 5. Geometrical changes along various courses of CO insertion reaction. (a) Numbers in parentheses represent the energies at each step relative to the starting complex **1** or **2**. Numbers without parentheses are geometrical parameters (Å and deg); underlined numbers are assumed and the rest are optimized values. (b) No energy minimum was obtained by the geometry changes of Scheme IVC and F. **9** and **12**, not being in local minimum, are less stable than **1** and **2** by ca. 100 and 96 kcal/mol, respectively. (c) Optimization was carried out in the following order; the orientation of CO and CH_3, the Pt–CH_3 bond distance, and then the positions of F and PH_3.

$\sim$ 110° is larger than 90°, this geometrical change shown in Scheme IVB apparently leads to **3**, and therefore, this course of reaction can be called the alkyl migration (see also Scheme III).

Scheme VI

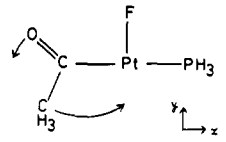

A further optimization without the constraint of ∠FPtP = 90° transforms **8** into **7**. Thus, the alkyl migration is likely to be combined with **3** → **5** transformation, leading directly to **5**.

The other course of reaction, C, shown in Scheme III was examined, where CH_3 and CO were placed in the same positions as courses A and B and the FPt(CH_3) angle was decreased keeping ∠FPtP $\sim$ 90°. This geometry change apparently leads to **4** as shown in Scheme IV, and therefore this course can be called the CO migration (see Scheme II). This geometry change is found to cause a significant destabilization, as shown by **9** in Figure 5, and is not likely to take place.

Next, the reaction starting from **2** will be examined. The most stable movement of F and PH_3 at step III is marked D, in Scheme IV and Figures 4 and 5, which requires an activation barrier of 54 kcal/mol. This movement of F and PH_3 should lead to **4**, and in fact, structure **10** resembles that of **4**. Thus, this course of reaction is called the CH_3 migration. Course E, in which the FPtP angle is opened as shown in Scheme IVE and therefore **5** is formed, needs a significantly higher potential energy of $\sim$70 kcal/mol (see Figure 4). The top of the potential barrier exists at around ∠FPtP = 120° (structure **11** in Figure 5). Since the C–C distance is longer than that of the $COCH_3$ group, this reaction course cannot be regarded as a CO migration followed by F migration but rather should be called the concerted movement of CH_3 and CO, like the course of reaction A. Finally, course F of Scheme IV was examined, in which the FPt(CO) angle was increased keeping ∠FPtP $\sim$ 90° to form **3**, as shown in Scheme IVF. This course, corresponding to CO migration, requires a very high barrier as shown by **12** of Figure 5 and is not likely to take place.

Figure 4 indicates that the CO insertion product **4** can easily suffer the reverse deacylation reaction and go back to **2** along path D shown in Figure 5; the CH_3 group can easily move to the vacant site in **4**, as shown in Scheme VI. Two possibilities exist to prevent deacylation. First, the dimer $Pt_2(\mu\text{-}F)_2(COCH_3)_2(PH_3)_2$ can be formed after **4** isomerizes to **3** or **5**. However, such isomerization requires a further potential barrier of 23 kcal/mol (Figure 3) and is not a likely process. Another possibility is to stabilize **4** by coordinating tertiary phosphine at the vacant site. It has been found experimentally that a rapid addition of tertiary phosphine causes a CO evolution to form *trans*-$PtX(R)(PR'_3)_2$ and that *trans*-$PtX(COR)(PR'_3)_2$ can be formed only when tertiary phosphine is slowly added to the equilibrium solution containing $PtX(CO)(R)(PR'_3)$ and $Pt_2(\mu\text{-}X)_2(COR)_2(PR'_3)_2$. **4** cannot form such a dimer, as described above. Via either way **4** does not appear to be stabilized, and the reverse deacylation is likely to take place in reaction course D. Since the other two courses, E and F, requires a very high potential barrier, we suggest that **2** cannot lead to any stable acetyl complex.

The conclusions of this section can be summarized as follows: (1) **1** gives **3** or **5** through the alkyl migration or the concerted movement of CH_3 and CO with simultaneous opening of ∠FPtP. (2) **2** gives **4** through the alkyl migration, but **4** cannot be stabilized and the reverse deacylation is likely to proceed easily. Thus, the CO insertion does not seem to proceed from **2**. (3) The CO migration is difficult, starting either from **1** or **2**.

Energetics and Change of Electronic Structure during the CO Insertion. Here, energetics of the CO insertion and changes of electronic structure are investigated in detail for the probable reactions **1** → **3** and **1** → **5**. As is shown in Figure 4, the CO insertion is endothermic; for **1** → **3**, ΔE = +50 kcal/mol, for **1** → **5**, ΔE = 34 kcal/mol. Endothermicity of the CO insertion has been experimentally reported for an Ir complex.[35a]

$$IrCl_2(CF_nH_{3-n})(CO)(PPh_3)_2 \rightarrow IrCl_2(COCF_nCH_{3-n})(PPh_3)_2$$

$$\Delta H^\circ = +7 - +20 \text{ kcal/mol}$$

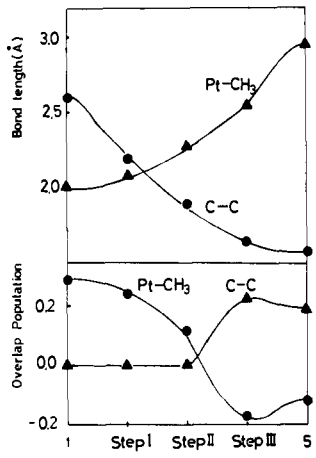

Figure 6. Changes in bond lengths and Mulliken populations during the CO insertion going from 1 to **5**.

The calculated activation barrier of ca. 60 kcal/mol for **1** → **5** and **1** → **3** is expected to be a substantial overestimate at this level of calculation. The experimental activation enthalpy ($\Delta H^{\ddagger}$) values for PtXR(CO)L are 18.3 kcal/mol (X = I, R = C_2H_5, L = PPh_3)[8a] and 19.4–21.4 kcal/mol (X = Cl, R = CH_3, L = $AsPh_3$)[7], and $\Delta H^{\ddagger}$ for $IrCl_2(CF_3)(CO)(PPh_3)$ is 42.5 kcal/mol.[35b] A part of the large discrepancies in both the activation energy and the endothermicity between calculation and experiments is due to the difference between PH_3 (calculation) and PPh_3 and $AsPh_3$ (experiments), for such bulky ligands would destabilize the four-coordinate starting carbonyl complex relative to the sterically less crowded transition state and final state. In fact, it has been argued that the bulkiness of ligands is an important factor for interconversion of an alkyl complex into an acyl complex.[36b,37]

Figure 6 gives changes of overlap populations and bond distances of two important atom pairs in the most probable reaction **1** → **5**. When CO and CH_3 groups approach to each other, the Pt–CH_3 distance increases and its overlap population decreases, becoming antibonding at step III. While the CH_3–CO distance gradually decreases from **1** to **5**, the increase of the C–C overlap population is rather sudden at step III, signaling the C–C bond formation. Thus, it can be said that the Pt–CH_3 bond is nearly broken and the C–C bond is almost fully formed at step III, the transition state region. In other words, the transition state of the CO insertion is product-like. Kampmeier et al. also has pointed out that the transition state of decarbonylation of $RhCl_2(COPh)(PPh_3)_2$ is an acyl-like complex.[36a]

Factors Determining the Course of Reaction. It is worthwhile to investigate why the alkyl migration but not the CO migration can proceed in the reaction systems starting from **1** and **2** and why the concerted migration can proceed starting from **1** but not from **2**.

Figure 5 shows that the motion of F^- and PH_3 from their original positions is small up to step II and suddenly becomes significant at step III, determining the course of reaction. Therefore we will concentrate on the motion of F and PH_3 in step III. Here we introduce a hypothetical reference structure III_0, in which CH_3 and CO are placed as in step III ($\angle CPtC = 39°$) but F^- and PH_3 ligands are placed as in step II ($\angle FPtP = 92°$, $\angle PPtC = 122.5°$, $\angle FPtC = 106.5°$). The structure III_0 lies in-between **8** and **9**.

The preference among courses A–F will be discussed on the basis of the orbital mixing scheme for different angular changes relative to the reference III_0. In Figure 7A, the MO diagram in the vicinity of HOMO and LUMO is shown for the reaction system **1**, as an example. The HOMO is the lone-pair orbital of the nearly formed CO···CH_3^- group, into which the more unstable $d_{x^2-y^2}$ mixes in phase and the more stable d_{xy} out of phase, as shown in Figure 8A. As shown in Figure 7B, HOMO is stabilized going to **7** and **8** from III_0 (i.e., easier reaction paths) but is destabilized going to **9**, the more difficult path. Thus, the choice of reaction paths seems to be determined by the behavior of HOMO of III_0. Apparently the stable positions of F^- and PH_3 are changed upon the formation of CH_3CO^- group, and they start to move to their new positions to restabilize the system. First, let us look at reaction system starting from **1** (see Figure 8A). When these two ligands

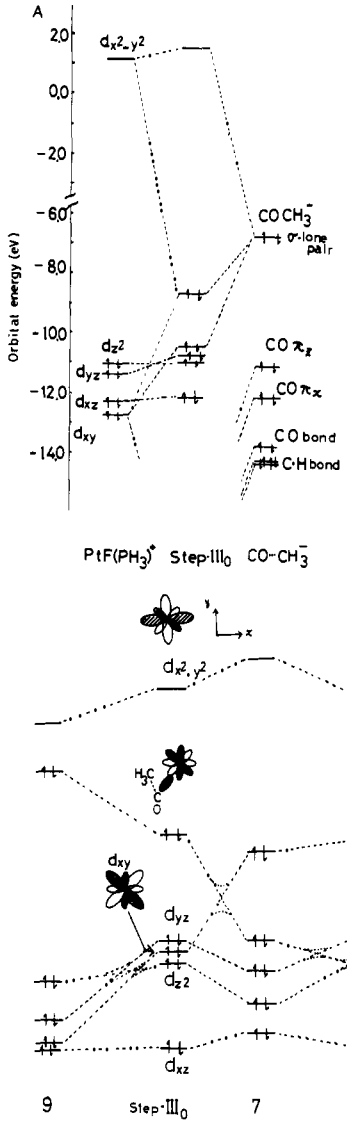

Figure 7. (A) Orbital correlation diagram in step III_0 between PtF-$(PH_3)^+$ + $COCH_3^-$ → $PtF(COCH_3)(PH_3)$. MO levels for the fragments are shifted by the electrostatic field of the partners. (B) Changes in MO energy levels caused by the movement of F and PH_3 from step III_0, as shown in Figure 5A and Scheme IVA–C.

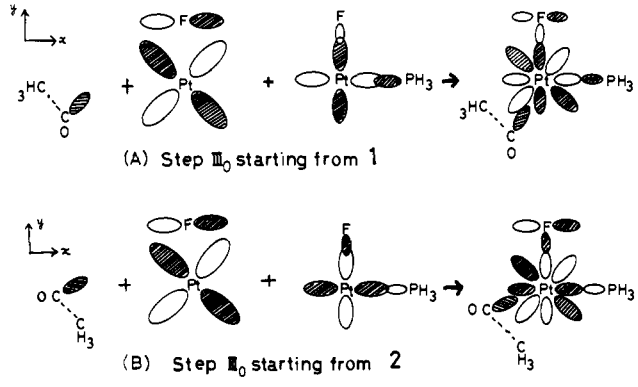

Figure 8. The lone-pair orbital of the nearly formed CO···CH_3^- mixed with Pt dπ and Pt dσ at step III_0.

(37) Barnard, C. F. J.; Daniels, J. A.; Mawby, R. J. *J. Chem. Soc., Dalton Trans.*, **1979**, 1331.

Scheme VII

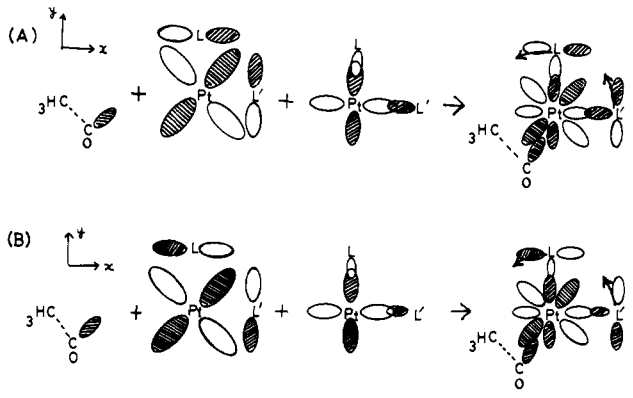

move along the arrows shown in Scheme IVA and B, the Pt–PH_3 bonding interaction becomes stronger. The geometry change B strengthens the Pt(d_{xy})–F($p\sigma$) bonding and the Pt(d_{xy})–F($p\pi$) antibonding interaction but reduces Pt($d\sigma$)–F($p\sigma$) antibonding interaction, whereas geometry change A strengthens the Pt(d_{xy})–F($p\sigma$) antibonding interaction and reduces the Pt(d_{xy})–F($p\pi$) and Pt($d\sigma$)–F($p\sigma$) antibonding interaction. Though this argument favors B slightly over A, B suffers from the steric repulsion between F^- and PH_3. Thus A and B should result in a similar degree of stabilization. The geometry change in Scheme IVC, however, enhances the Pt(d_{xy})–PH_3(σ) lone-pair antibonding interaction, without strengthening the Pt–F bond. Thus this movement would destabilize the reaction system, making the corresponding reaction path C of Figures 4 and 5 more difficult.

Now the reaction system from **2** will be examined. Figure 8B suggests that in the geometry change in Scheme IVD, the Pt(d_{xy})–F($p\sigma$) and Pt(d_{xy})–PH_3(σ) lone-pair bonding interaction increases, whereas the Pt($d\sigma$)–F($p\sigma$) and Pt($d\sigma$)–PH_3(σ) lone-pair antibonding interaction decreases. Thus the corresponding reaction course D (**2** → **4**) of Figures 4 and 5 is a favorable path. The geometry change of Scheme IVE should enhance both the Pt(d_{xy})–PH_3(σ) lone-pair antibonding interaction and the Pt(d_{xy})–Fp(σ) bonding interaction, whereas the change of Scheme IVF enlarges the Pt(d_{xy})–PH_3(σ) lone-pair antibonding interaction as well as the Pt(d_{xy})–F($p\sigma$) antibonding interaction. Since PH_3 interacts with Pt more strongly than F, both movements E and F should result in destabilization of the reaction system. This explains why the corresponding reaction courses E (**2** → **5**) and F (**2** → **3**) of Figures 4 and 5 are difficult.

In conclusion, we have explained the choice of courses of reaction based on the orbital mixing at step III_0 where the C–C bond is almost formed between CH_3 and CO; **1** → **3**, **1** → **5**, and **2** → **4** are easy process, because the Pt–PH_3 bond becomes strong due to this orbital mixing, but **1** → **4**, **2** → **3**, and **2** → **5** are difficult process, since the Pt–PH_3 bond becomes weak due to this orbital mixing.

Finally, we will discuss the possibility of the CO migration mechanism. For CO migration to proceed, the ligands have to move in the directions shown in scheme IV, C and F. If the $d\pi$ orbital is less stable than the CO···CH_3^- lone-pair orbital, the $d\pi$ mixes with the lone pair as shown in Scheme VII, and therefore, the geometry change of Scheme IVC, shown as arrows in Scheme VII, can proceed; i.e., the CO migration becomes possible. The π-acceptor ability of ligands should facilitate the CO migration (Scheme VIIA), while the π-donor ability should retard it (Scheme VIIB). Thus, the required conditions for CO migration may be that the central metal has enough Lewis basicity and its $d\pi$ is unstable relative to the lone pair of CO···CH_3^- and that the ligands are π-acceptors.

Concluding Remarks

Structures of Pt(CH_3)F(CO)(PH_3) and Pt($COCH_3$)F(PH_3) were optimized by means of an ab-initio MO method and energy gradient techniques. The optimized bond lengths agree well with experimental values, except for the Pt–F bond distance which was calculated too short. An emphasis of the study is placed on the three-coordinate d^8 complex Pt($COCH_3$)F(PH_3). The relative stability of isomers and the potential barrier for isomerization were investigated; the Y-shaped complex is unstable and isomerizes to a T shape with no barrier. The relative stability of T-shaped complexes was explained by the trans-influence effect. All possible courses of the CO insertion reaction, including CH_3 migration, CO migration, and the concerted migration of CO and CH_3 with ∠FPtP opening were examined. In both isomers **1** and **2** of Pt(CH_3)F(CO)(PH_3), CH_3 migration can take place but CO migration cannot. The concerted migration is easy for **1** but difficult for **2**. These results support previous experimental proposals. The factors determining the courses of reaction are also explained; CO migration in both **1** and **2** as well as the concerted migration in **2** increase the Pt–F and Pt–PH_3 antibonding interaction, and consequently, these courses of reaction are unfavorable. The orbital mixing between Pt d_{xy}, $d_{x^2-y^2}$, and the lone-pair orbital of $COCH_3$ show how the choice of reaction courses is made. A condition where the CO migration may become possible is also proposed.

Acknowledgment. The present research is in part supported by the Joint Studies Program (1981–1982) of the Institute for Molecular Science and by a Grant-in-Aid for Special Project Research on innovative studies on highly selective synthesis. The numerical calculations have been carried out at the Computer Center of the Institute for Molecular Science.

Registry No. 1, 84960-54-3; 2, 85026-72-8; 3, 84960-55-4.